

Ishtiaq A. Chaudhry · S. Zhong

## A single circular synthetic jet issued into turbulent boundary layer

Received: 9 April 2013/Revised: 1 February 2014/Accepted: 20 February 2014/Published online: 5 April 2014  
© The Visualization Society of Japan 2014

**Abstract** An experimental investigation has been undertaken to study the behaviour of a single circular synthetic jet issued into turbulent boundary layer produced on a flat plate in cross flow. At the given free-stream conditions, the jet is also issued into laminar boundary layer so that an effective evaluation on the interaction of the vortices with the changing boundary layer could be made. The flow visualization technique is used in conjunction with the stereoscopic imaging system to reveal a unique quasi three-dimensional recognition of the vortices formed in either type of boundary layer under varying synthetic jet actuator (SJA) operating conditions. Firstly, the laminar boundary layer is produced on the flat plate with zero pressure gradient and later on the same boundary layer is triggered to turbulence using a trigger device. The free-stream conditions are justified by PIV measurements, in that the velocity profiles are drawn at given streamwise locations for both laminar and turbulent boundary layers. The parametric map is given to identify and bound the SJA operating parameters to produce the explicit vortical structures at the given conditions.

**Keywords** Streamwise vortices · Synthetic jet actuator · Wall shear · Tilted vortex rings

### List of symbols

$D_c$	Cavity diameter, mm
$L$	Dimensionless stroke length
$U$	Characteristic velocity, m/s
$y$	Normal distance from wall, mm
$\delta$	Boundary layer thickness, mm
$\rho$	Fluid density, kg/m <sup>3</sup>
$Re_L$	Reynolds number based on dimensionless stroke length
$f$	Diaphragm oscillation frequency, Hz
$St$	Strouhal number
$x$	Streamwise distance, mm
$z$	Spanwise distance from centerline, mm
$c_f$	Skin friction coefficient
$\Delta$	Diaphragm peak-to-peak displacement, mm

## 1 Introduction

Crook and Wood (2001) implemented an array of jets upstream of separating line in a turbulent boundary layer produced on the surface of a circular cylinder and found that the separation line was pushed downstream considerably when the actuators were active. Zhong et al. (2005) undertook dye visualization technique to study the formation of a single circular synthetic jet in a laminar boundary layer and discussed the propagation of various vortical structures downstream. Zhong concluded that the interaction between the streamwise pair of vortices and the near wall fluid is rather complex, varying from hairpin vortices to tilted vortex rings that penetrate the boundary layer to a larger extent. In conclusion, Zhong hypothesized that the hairpin vortices are more effective towards separation delay because of their tendency to remain within boundary layer for a larger range of jet to free-stream velocity ratio. The numerical simulation studies of Zhou and Zhong (2008) also confirmed the presence of hairpin-type structures and further observed that the hairpin legs trailing along the wall also induce a pair of streamwise vortices with opposite sense of rotation. The hairpin legs and the induced streamwise vortices together create a downwash which ultimately brings high speed fluid from the outer part of the boundary layer to the near wall region.

Nevertheless, one unique attribute of SJA is that they can be operated on a wider range of operating parameters to produce a range of vortical structures without any involvement of complex driving mechanism. However, the previous reported work on SJA revealed that the operating parameters were set by hit and trial, as the specific vortical structures were produced under varying operating conditions. As a result, the operating conditions such as jet to free-stream velocity ratio were varying from one experiment to other and the subsequent effectiveness of the jet has been observed to fluctuate in an unpredictable manner. Secondly, to simplify the measurements, most of the previous work on synthetic jets was undertaken in a laminar boundary layer and attempts were made to co-relate the results with the turbulent boundary layer. Although for the boundary layer separation control, the effectiveness of the SJA has already been demonstrated experimentally by many laboratory-based investigations, yet the understanding of the fluid mechanics involved in the interaction of the vortical structures with the boundary layer fluid needs further investigations. Furthermore, the interaction mechanism of the synthetic jet with the separating flow especially in turbulent boundary layer still remains far beyond fully understood. The present work involves in-detail experimental investigation of the evolution of vortical structures in the turbulent boundary layer. The characteristics of vortical structures are compared in either type of boundary layer at given free-stream conditions. Finally, for a given incoming flow conditions, the operating parameters are specified to produce the desired vortices with explicit characteristics to deliver the best possible streamwise control effects.

## 2 Experimental set up

A bench-top SJA rig available at Pariser hydraulics laboratory at the University of Manchester is used to facilitate a parametric investigation under a range of SJA adjustable operating parameters. The synthetic jet actuator consists of a circular cavity and a rubber diaphragm sandwiched between two rigid steel disks. The top side of the cavity is enclosed by the diaphragm, while the bottom side is formed by the orifice plate (Chaudhry and Zia 2012). The thickness of the orifice plate is exactly the same as that of the test plate i.e.,  $h = 5$  mm. The diaphragm is connected with the shaker by a steel rod. The shaker is driven by an amplifier and the input signal to the amplifier is a sinusoidal signal generated by the DAQ card. The Monitron eddy current displacement sensor consisting of a probe (MTN/EP080) and a driver (MTN/ECPD) is used to measure the displacement of the diaphragm. The sensor works in conjunction with a small metallic target fixed on a circular perspex disk. Facing upward right onto the target, the sensor probe is fixed on a separate rectangular perspex strip firmly held affixed on the frame (Chaudhry and Zhong 2012).

Use is made of a tilting water flume having the maximum achievable free-stream velocity of 0.4 m/s. In the test section of the flume to keep the plate well submerged, a specific water level is maintained with a constant free stream velocity of 0.1 m/s. The test plate is constructed from a 5 mm thick sheet of aluminum (Al HE30) (Fig. 1) with a super elliptical leading edge with 1:5 nose thickness to length ratio to avoid any separation and pre-mature transition at the leading edge. The orifice ( $D_o = 5$  mm) is located at 0.7 m ( $=140 D_o$ ) aft of the leading edge along the centre-line of the plate. This location is chosen to provide an adequate far downstream distance from the leading edge to allow sufficient build-up of boundary layer thickness ( $\sim 6 D_o$ ) and a necessarily needed usable width of the plate. A Hitachi KP-F120 partial scan CCD camera with a maximum available resolution of  $1,260 \times 1,040$  pixels is used to capture the dye pattern produced from two

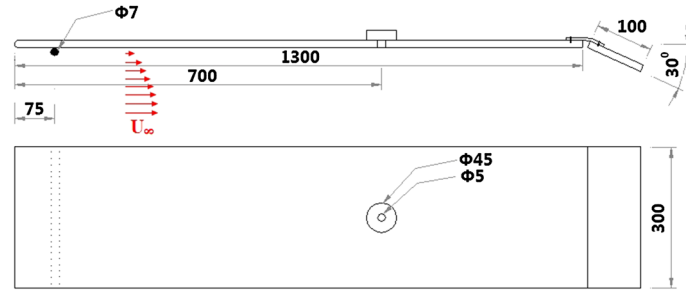


Fig. 1 Schematic of the test plate (dimensions in mm)

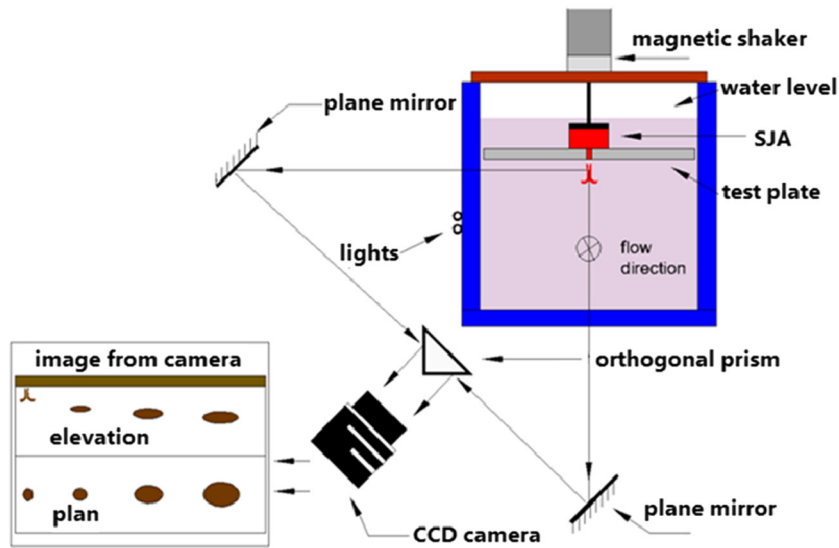


Fig. 2 End-view of the stereoscopic imaging system

orthogonal views simultaneously at a frame rate of 30 fps, providing a quasi three-dimensional visualization of the jet. Using a combination of two plane mirrors with an orthogonal prism, a stereoscopic imaging system is set up (Fig. 2) to facilitate the capture of both views simultaneously.

### 3 Parametric analyses

Glezer (1988) described the formation pattern of the vortex ring by introducing cylindrical–slug model in which a cylindrical volume of fluid moves at constant velocity ' $U_o$ ' for a time ' $T$ ' through a circular orifice of diameter ' $D_o$ '. From the basis of the dynamic incompressible flow model established by Tang and Zhong (2006) in which the dye in the cavity is assumed to be incompressible, the time averaged blowing velocity over the cycle is given by

$$\bar{U}_o = \frac{1}{T} \int_0^{T/2} \tilde{u}_o(t) dt = f \Delta \left( \frac{D_c}{D_o} \right)^2 \quad (1)$$

The stroke length (length of the fluid slug) is now defined as

$$L_o = \int_0^{T/2} \tilde{u}_o(t) dt \quad (2)$$

$$L = \frac{L_o}{D_o} = \frac{\bar{U}_o T}{D_o} = \frac{\bar{U}_o}{f D_o} \quad (3)$$

' $f$ ' is the excitation frequency and can be non-dimensionalised in Strouhal number such as

$$St = \frac{f D_o}{U_o} = \frac{1}{L} \quad (4)$$

It is rather feasible to relate the Reynold number with the stroke length such as

$$ReL = \frac{\bar{U}_o L_o}{\nu} = Re \frac{L_o}{D_o} = Re.L \quad (5)$$

For incompressible isothermal flow with external pressure remains constant, the boundary layer thickness is non-dimensionalised by the orifice diameter

$$d = \frac{\delta}{D_o} \quad (6)$$

The operating parameters are extended to be related with free-stream velocity  $U_\infty$ . Therefore, in addition to the key dimensionless jet parameters (i.e.,  $L$  and  $Re_L$ ), the jet velocity-to-free-stream velocity ratio, VR, need to be considered and is given by

$$VR = \frac{\bar{U}_o}{U_\infty} \quad (7)$$

'VR' characterizes the relative strength between the jet and the free-stream velocity and ultimately characterizes the jet trajectory. The smallest ' $f$ ' used in the experiments is 1 Hz which should be at least two times than that of the T-S wave not to affect the stability of the boundary layer. However, the stability is confirmed by calculating the indifference ' $Re$ ' to be  $\approx 383$  which is not exceeding the minimum value of 520.

## 4 Results and discussion

### 4.1 Test conditions

In the test section of the flume, the flow is set to be two-dimensional and it is confirmed firstly by measuring the streamwise and spanwise velocity profiles using a Nixon Streamflow vane anemometer as shown in Fig. 3. Secondly, by performing the PIV measurements, the boundary layer velocity profiles are drawn at various streamwise locations deemed critical for measurements and with no slip condition at the wall, a good match with Blasius solution is met. A good agreement with the Blasius profile confirms the zero pressure gradient nature of the laminar boundary layer at all the given locations. For turbulent boundary layer, the same laminar boundary layer is triggered to turbulence by a trigger device placed at a specific distance from the leading edge. The size in terms of diameter and the location of the device from the leading edge is specified by calculating the Reynold's number based on the momentum thickness (Chaudhry and Zhong 2013).

### 4.2 Synthetic jet interaction with boundary layer

Figure 4 shows the vortex formation both for laminar (A) and turbulent (B) boundary layers. For hairpins, the front tip is referred to as the vortex head, while the trailing following portion that remains relatively closer to the wall is termed the hairpin legs (Fig. 5). The vortex legs become thinner and relatively longer as it travels farther away because of the prevailing flow momentum and the influence of shear. A vortex travelled far away from the orifice is a decaying vortex with the initial vorticity of the hairpin diffusing in the presence of viscosity. Similarly, a vortex nearer to the orifice appears to be a growing vortex that

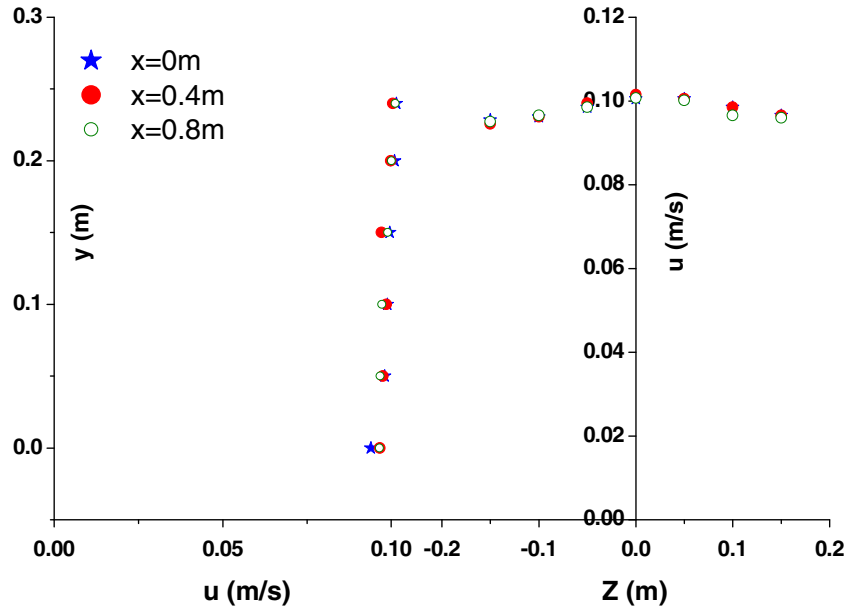


**Fig. 3** Velocity profiles at various locations in the flume test section

interacts strongly with the near wall surface fluid resulting in a strong momentum exchange. Figure 4Aa (plan) reveals the development of dye concentration laterally alongside each vortex leg and are called longitudinal vortices or secondary streamwise vortices. The formation of longitudinal vortices is the process of intensification of the secondary vortical structures due to the velocity gradients generated by the intruding flow (Acarlar and Smith 1987).

In the boundary layer, the vortex penetration rate is related to the stroke length value as evident from Fig. 4Ab where the vortices produced at relatively higher stroke length eventually push the hairpin head out of the boundary layer. The increased  $Re_L$  results in the enhanced vortex strength, further increasing the induced velocity generated between the head and the counter-rotating legs. As the stroke length increases the hairpins undergo greater streamwise stretching (Fig. 4Ab) and thus result in the creation of what are usually called kinks somewhere in the middle of the legs as they gradually tend to feeble by virtue of imparting more energy to the vortex head. This eventually results in the formation of kinks and normally this stage is considered the in-between form between the hairpins and the stretched vortex rings (SVR).

Haidri and Smith (1994) illustrated the transformation of an initial hairpin to a turbulent spot structure through systematic generation of new vortices. In this work, the boundary layer is triggered intentionally to study the evolution of vortices in the turbulent boundary layer where the hairpins are found to be strongly interactive, demonstrating remarkable reproductive characteristics. The hairpin generated as the result of the injection is called the primary vortex and any additional vortices formed by the interaction of the primary vortex with the local fluid are termed as secondary vortices (Fig. 4Bb). At lower stroke length, the secondary vortices are not quite discrete but only appear to be distinct at relatively higher stroke length (Fig. 4Bb,  $L = 3.6$ ). It is evident that the vortex structure in laminar boundary layer remains quite distinct, symmetric and repetitive. As a result of the large number of competing vortices and local disturbances, the vortices in the turbulent boundary layer are asymmetric or 'single-legged' hairpins generally described as 'quasi-streamwise vortices' i.e., vortices that consist principally of a convected section of streamwise vorticity (Robinson 1991). Secondly (Fig. 6), they are not essentially repetitive unlike their symmetric counterparts in that the following injection cycle does not produce the same asymmetric vortex pattern essentially symmetric to those produced in the previous cycle. At  $L = 2.2$  (Fig. 4Ba), the more prominent difference is that the vortices are fairly immature so require relatively higher stroke length and VR to become stable. Furthermore, the immature vortices interact with the local turbulence and become vulnerable a lot earlier to distort and eventually decay to zero existence (Fig. 4Ba). In the near wall region, the velocity gradient is lot more severe and so is the shear which inhibits the vortex development. In the near wall region the turbulence is rigorous than the outer part of the boundary layer. Therefore, as anticipated, the effect of this local turbulence is more prominent on the development of hairpins compared to those vortices which

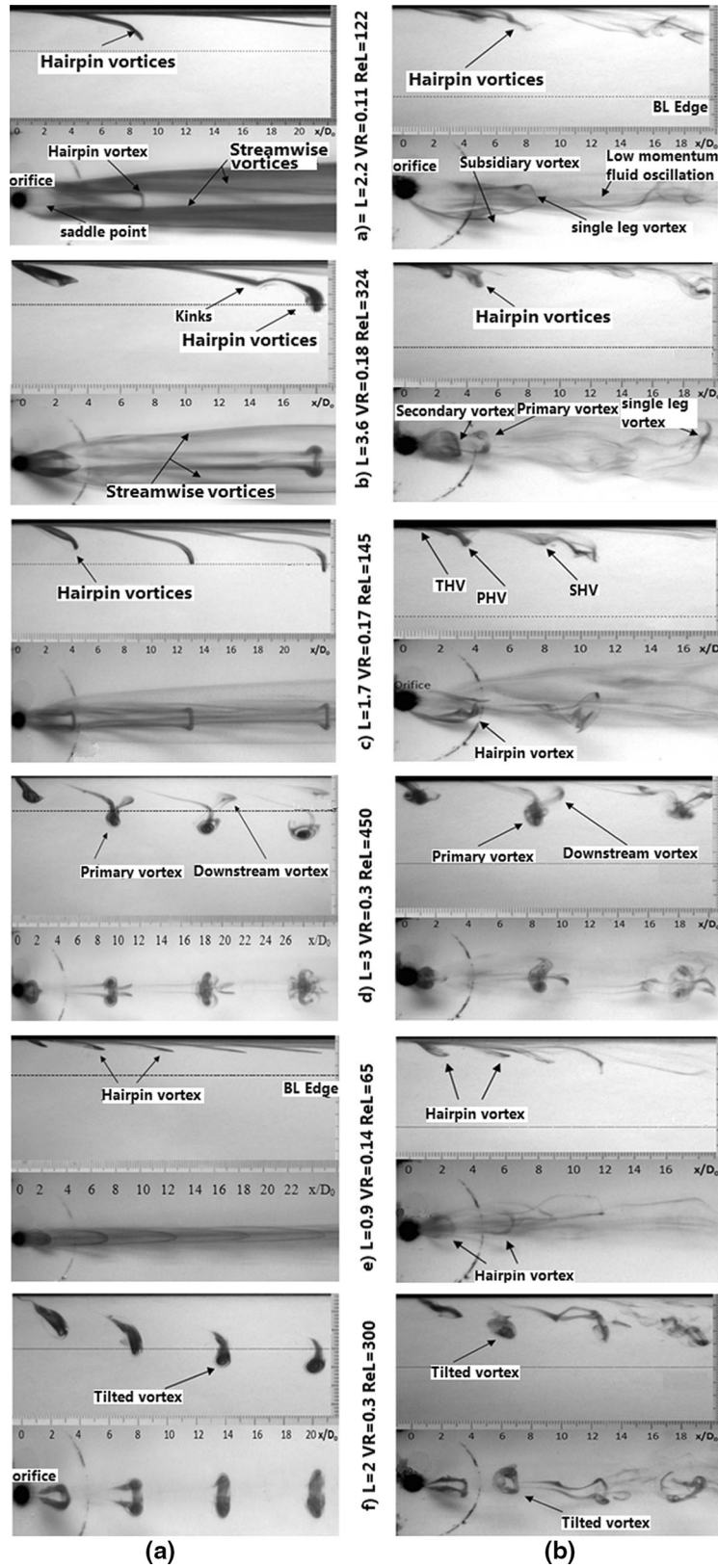
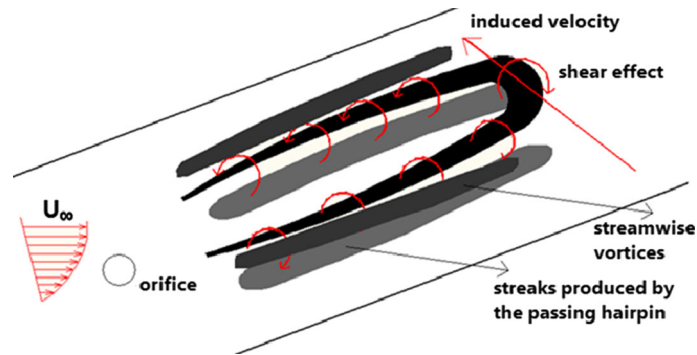
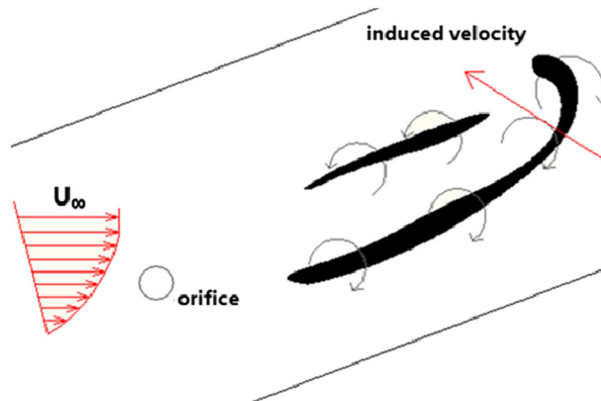


Fig. 4 Vortex formation A laminar BL, B turbulent BL



**Fig. 5** A hairpin in the laminar boundary layer



**Fig. 6** A hairpin in the turbulent boundary layer

have been produced at larger stroke length. The turbulence seems to dominate the induced velocity causing the oscillation of low-momentum fluid (Fig. 4Ba) in a spanwise plane, and the presence of the distinct ridges (Fig. 4Bb), ostensibly appear due to the development of secondary structures. The low-momentum regions (4Bb) oscillate in the cross-stream plane, similar to the behaviour of turbulent low-speed streaks. A considerable lift up of streamwise vortices (Fig. 4Ba) seems more likely to a violent eruption of fluid away from the wall.

The process of development as it travels downstream undergoes the vortex regeneration both laterally and in the wake of the primary vortex and that eventually leads to the continued growth of turbulence in the primary vortex which ultimately results in the distortion of the primary vortex. Owing to turbulence and the viscous effect, the secondary vortex separates from the primary vortex and travels independently farther downstream and decays far earlier than the primary structure. Three-dimensional Biot–Savart calculations (Hont and Walker 1987; Smith et al. 1991) of the motion and deformation of a single vortex line indicate the development of subsidiary vortices by lateral inviscid deformation. The formation of the subsidiary vortices is quite distinct (Fig. 4Ba, Bb), which is actually the result of the inviscid deformation of the collective vortex lines comprising the primary vortex. For a strong primary structure that remains in proximity to the surface, a localized viscous growth of wall fluid initiates that eventually focus rapidly and ‘erupt’ from the surface. It generates a spire of fluid that subsequently interacts with the outer flow and this process is commonly known as an inviscid–viscous interaction (Peridier et al. 1991). At relatively low stroke length (Fig. 4Bb) where there is no prominent appearance of such vortices due to less rotation of the vortex head that eventually considered not sufficient to impose a considerable local transient 3-D streamwise adverse pressure gradient.

At  $St = 0.1$  (Fig. 4c, d), the spacing between the adjacent vortices is reduced considerably because of an increase in the Strouhal number. The inclination of the vortex from the wall is found to be varying and is a function of the resultant of the opposing effect of self-induced velocity that moves the leading portion of the



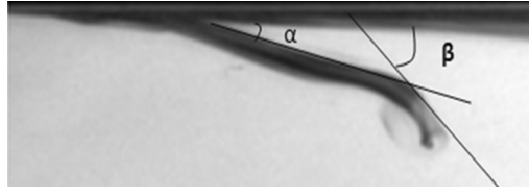


**Fig. 7** Angle associated with hairpin vortex

hairpin away from the wall and the presence of shear in the boundary layer that tends to attract them back to the wall. For Fig. 4Aa, Ac, the hairpin head for the latter case moves along a steeper path because of the larger self-induced velocity. This asymmetry in turbulent boundary layer (Fig. 4Bc) gives rise to the earlier formation of what is called secondary (SHV), tertiary (THV) and downstream hairpin vortices (DHV) (Zhou et al. 1999). The secondary and tertiary vortices are quite prominent, but the downstream vortices become distinctive at a bit further stroke length (Fig. 4Bd). The angles described by the vortex legs ( $<\alpha$ ) and head ( $<\beta$ ) examine the projected geometric changes during the hairpin proceedings and formation (Fig. 7).

At  $St$ . 0.15, the vortices are agglomeration of weak hairpins that remain embedded closer to the wall and are analogous to quasi-steady, streamwise vortex pair. The relative dominance of the mean shear over self-induction causes the insignificant lift up of the vortex head away from the wall deterring the evolution of the head such that the hairpins appear to be more parabolic in shape. Adjacent vortices are closer and relatively easier to compare the effect of turbulence on each individual structure. Furthermore (Fig. 4Be), it appears that the displacement between adjacent vortices is not regular owing to irregular turbulence and customary uneven spanwise local velocity factor. At increased stroke length (Fig. 4Af), the vortices tend to protrude out of the boundary layer far earlier and subsequently undergo less streamwise stretching due to shorter residence time in boundary layer. The vortex legs observed to peter out completely giving rise to the new vortex structure called the tilted vortices. Owing to the rotation of the vortex head, the small tail appearing nearer to the orifice ultimately merged into the head that by now entrains the fullest energy of the vortex.

### 4.3 Near wall evolution

In the near wall region, the evolution of vortical structures is presented in Fig. 8. The image sequence is not taken exclusively at the same matching phase of the cycle, but at arbitrary instant when the structure is relatively distinguishing to illustrate the ensuing roll-up and break-up process. At low  $Re_L$  both the counter-rotating legs of the weak hairpin ( $T_3, T_4$ ) appear to remain under rather fluctuating shear with fairly uneven magnitude leaving both the legs follow quite a swirling course downstream. They appear to be completely asymmetrical ( $T_4$ ) where both the legs remain independent from each other in the absence of a distinctive vortex head vulnerable to decay at much faster rate. At relatively increased VR (Fig. 8b) where the  $Re_L$  has been enlarged significantly the vortex appears to exhibit a considerable strength and a significant roll-up on the downstream branch, ( $T_2, T_3$ ).  $Re_L$  has been increased to a greater extent compared to VR and  $L$  to demonstrate that the roll-up is more affected by  $Re_L$ . As such, these structures are actually the intermediate forms of hairpins and tilted vortex rings and have been named stretched vortex rings in earlier literature because of their tendency to differ from hairpins in that they are more likely to accommodate the vorticity in the head rather than the counter-rotating vortex legs. Secondly, the upstream branch is more affected by the resident vorticity in the boundary layer than the effect of suction. However, towards the end of their complete formation they exhibit more or less the shape of hairpins.

Figure 8c shows vortices produced at larger velocity ratio but smaller Reynolds number compared to Fig. 8b where the effect of suction stroke appears to be subdued compared to the effect of resident vorticity as the upstream branch does not remain completely restrained. The vortex seems to undergo larger radial spread because of the strong interaction with 3-D turbulence and subsequently it experiences a considerable tilting clockwise in the normal plane as the upstream branch has been lifted towards the wall while the downstream branch has been pushed away from the wall. The radial spread is a distinctive characteristic of the vortex in turbulent boundary layer, whereas the tilting development is similar as in laminar boundary layer. In laminar boundary layer at low VR, it takes quite a while depending upon the magnitude of VR for a vortex to develop into a turbulent phase. However, in turbulent boundary layer, the streamwise distance becomes fairly short, not more than  $5D_o$  for a vortex to develop into a turbulent structure. Although at higher



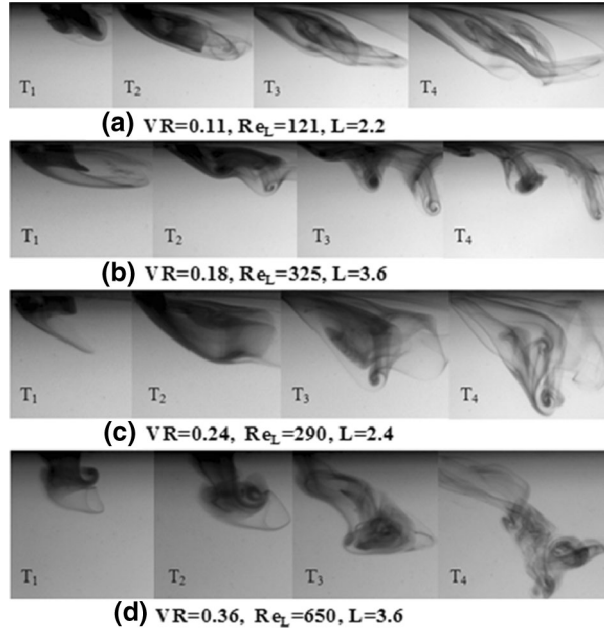


**Fig. 8** Vortex structures at various operating parameters

VR, the vortex appears to exhibit transition earlier, yet its ability to resist to the influence of the local turbulence seems to enhance a great deal and it behaves more likely as in the laminar boundary layer.

## 5 Parametric mapping

Based on the present observations and the previous experimental, analytical or numerical studies, it is inferred that the SJA effectiveness based on the other parameters could be summarized as

$$\text{SJA effectiveness} = f(L, Re_L, VR, d, c_f) \quad (8)$$

The SJA operating parameters at given free-stream conditions need to be confined to establish the domain of non-dimensional parameters at which the particular structures are formed or transformed. Towards establishing such domain, all the test cases undertaken are categorized in accordance to the parameters namely the velocity ratio 'VR', stroke length 'L' and Reynolds number based on stroke length ' $Re_L$ '. All these parameters are defined as previously and the remaining two parameters in (8) namely ' $d$ ' and ' $c_f$ ' remain unchanged throughout this work thus the reason of not including them in parametric mapping.

For the formation of each type of vortices, the threshold values of the operating parameters need to be confined to establish the range of conditions that ensures the evolution of particular structures for potential flow separation control. Towards establishing that range, all the test cases undertaken were categorized in accordance to the parameters given in (8). It is more reasonable to relate Strouhal number or the operating frequency with the corresponding stroke length since the frequency seems to influence the vortical structure directly with respect to stroke length. So, it is deduced that it is more reasonable to involve the operating frequency directly in parameter space (Fig. 9b). One of the hindrances to the mapping of vortex structures in turbulent boundary layers is that the vortical structures are not rigorously distinctive as in laminar boundary layer so it is not that straightforward to mark the threshold on the formation or demise of each structure, yet a moderate attempt is made to categorize the structures accordingly. In the first case, 'VR' is plotted against 'L' (Fig. 9a) where  $St$  is the gradient of VR–L. The blue lines mark the boundary or limit the different type of structures. Certainly, there is always an area of overlaps in-between the process of formation. Secondly, the initiation of the pattern of any new structure is always a gradual and steady course which could not be limited by a single line. The range of 'VR' and 'L' is reduced considerably in turbulent boundary layer to a noticeable extent because of the fact that the vortices produced at lower velocity ratio become distorted far earlier owing to turbulence and the local velocity perturbation within the boundary layer. For stretched

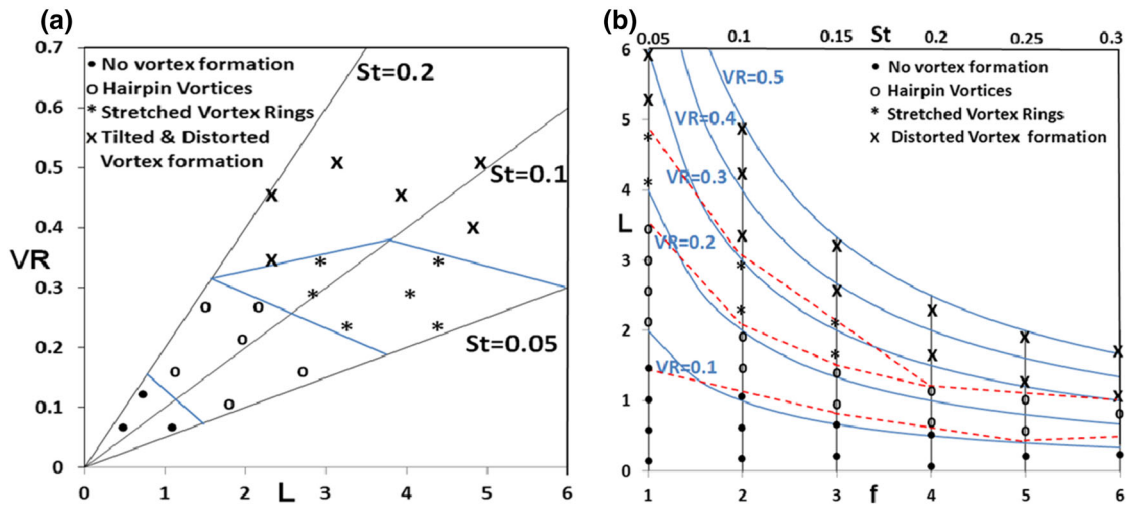


Fig. 9 Parameter space for various vortical structures for turbulent flow

vortices the range of VR is smallest at highest Strouhal number ( $St = 0.2$ ) since the hairpins are directly transformed to tilted or distorted structures. For synthetic jet effectiveness, it is believed that when increase in vortex strength is desired i.e., increase in ' $Re_L$ ' both VR and  $Re_L$  should not be too high such that vortices penetrate out from the boundary layer.

## 6 Conclusions and summary

In either type of boundary layer, three different types of vortical structures have been produced namely hairpin vortices, stretched vortex rings and tilted vortices. At higher velocity ratio and stroke length, the vortical structures in turbulent boundary layer resist the turbulence to a larger scale and behave more likely as their counterparts in laminar boundary layer. Tilted and distorted vortices are formed beyond stretched vortex rings when the SJA is operated at further higher stroke length and velocity ratio and are least likely to remain within the boundary layer. The tilted vortices seem to be more effective towards flow separation control although the primary vortex tends to protrude out of the boundary layer. However, their tendency to generate the trailing secondary and tertiary vortices that essentially remain within the boundary layer make them desirable structures towards potential flow separation control. The hairpins on the other hand are produced at the lowest possible velocity ratio and stroke length and hence the active flow control device consumes the minimum input energy. The hairpins produced at relatively larger Strouhal number seem to affect the boundary layer profile with rather continuing effect and their tendency to remain within the boundary layer yield a far more enhanced near wall fluid mixture. Therefore, the hairpins are considered to be the most effective structures to be issued into the boundary layer for maximum flow control effect, hence the need to operate the SJA at  $0.4 < VR < 0.5$ .

**Acknowledgments** The first author would like to thank University of Engineering and Technology Lahore, Pakistan to fund for his PhD studies and the moral support. Thanks to Dr. Zhang, S. for his valuable assistance to build the rig for the experimental work.

## References

- Acarlar MS, Smith CR (1987) A study of hairpin vortices in a laminar boundary layer; (P2) hairpin vortices generated by fluid injection. *J Fluid Mech* 175:43
- Cater JE, Soria J (2002) The evolution of round zero-net-mass-flux jets. *J Fluid Mech* 472:167–200
- Chaudhry IA, Zhong S (2012) Understanding the interaction of synthetic jet with the flat plate boundary layer. In: International conference on advanced research in mechanical engineering (ICARME), Trivandrum, India
- Chaudhry IA, Zhong S (2013) The evolution of synthesized vortices in turbulent boundary layer. *J Turbul* 14(10):1–18
- Chaudhry IA, Zia RT (2012) PIV investigation into the evolution of vortical structures in the zero pressure gradient boundary layer. *World Acad Sci Eng Technol* 60(71):27–33

- 
- Clauser FH (1956) The turbulent boundary layer in advances in applied mechanics, V, vol IV. Ac. Pr, New York
- Crook A, Wood NJ (2001) Measurements and visualisations of synthetic jets. In: Proceedings of 39th AIAA aero sciences meeting and exhibit, Reno, NV, USA, Paper 2001-0145
- Glezer A (1988) The formation of vortex rings. *Phys Fluids* 31(9):3532–3542
- Glezer A, Amitay M (2002) Synthetic jets. *Annu Rev Fluid Mech* 34:503–529
- Haidari AH, Smith CR (1994) The generation and regeneration of single hairpin vortices. *J Fluid Mech* 277:135–162
- Hont L, Walker JD (1987) An analysis of the motion and effects of hairpin vortices. Tech. Rep. FM-11, Department of M.E. and Mech., Lehigh University, Bethlehem, PA
- Peridier VJ, Smith FT, Walker JDA (1991) Vortex-induced boundary-layer separation (Part 2) unsteady interacting boundary-layer theory. *J Fluid Mech* 232:133–165
- Robinson SK (1991) Coherent motions in the turbulent boundary layer. *Annu Rev Fl Mech* 23:601–639
- Smith CR, Walker JD, Haidari AH, Sobrun U (1991) On the dynamics of near-wall turbulence. *Phys Sci Eng* 336(1641):131–175
- Tang H, Zhong S (2006) Incompressible flow model of synthetic jet actuators. *AIAA J* 44(4):908–912
- Zhong S, Millet F, Wood NJ (2005) The behaviour of circular synthetic jets in a laminar boundary layer. *Aeronaut J* 109(1100):461–470
- Zhou J, Zhong S (2008) Numerical simulations of the interactions of circular synthetic jets with a boundary layer. *Comput Fluids* 38:393–405
- Zhou J, Adrian RJ, Balachandar S, Kendall TM (1999) Mechanisms for generating coherent packets of hairpin vortices in channel flow. *J Fluid Mech* 387:353–396